1.Report No. TxDOT 4172 -1	2. Government Accession No.	3. Recipient's Catalog No.
4. Title and Subtitle Development of a Radar System for the Non-Destructive Measurement of Concrete Thickness		5. Report Date Feb. 2001 6. Performing Organization Code
7. Author(s) Richard Liu, Xuemin Chen, Jing Li, Huichun Xing, Renyue Liang		8. Performing Organization Report No. 4172-1
9. Performing Organization Name and Address Department of Electrical and Computer Engineering University of Houston 4800 Calhoun Rd. Houston, TX 77204-4793		10. Work Unit No. 11. Contract or Grant No. Project No. 0-4172
12. Sponsoring Agency Name and Address Texas Department of Transportation Research and Technology Implementation Office 4000 Jackson Av. Building 1 Austin, TX 78731		13. Type of Report and Period Covered Final Report April 1 – August 31, 2000 14. Sponsoring Agency Code

15. Supplementary Notes: Research performed in cooperation with the Texas Department of Transportation and the U.S. Department of Transportation, Federal highway Administration. Research project title: Development of a Radar System for the Non-Destructive Measurement of Concrete Thickness

16. Abstract:

This project is based on the previous research (0-1828 "Feasibility Study on Non-destructive Testing Technique to Measure PCC Pavement Thickness"), which provided information and a rudimentary radar system that may be able to be used to measure concrete pavement thickness during the curing stage. The technique utilizes a ground couple, pulse wave radar system. However, the system needs further improvement to be useful in the field. In this study, new pulse generator and new antennas are developed. The software of information extraction and thickness calculation is established. Concrete slabs of different thickness are constructed and used to testify the system. The experimental results on the slabs in the lab and on the field are presented. The tested results show that the thickness of concrete slabs can be determined non-destructively in a few milliseconds with an accuracy of 0.5 inches. The range of the thickness measurement reaches 16.5 inches without steel rebars. The developed technology can also be applied to the asphalt pavement for thickness measurement.

17. Key Words Pavement thickness, Dielectric constant, weak signal extraction, TEM horn antenna, Pulse generator	18. Distribution Statement No restrictions.		
19. Security Classif. (of this report) Unclassified	20. Security Classif. (of this page) Unclassified	21. No. of Pages 29	22. Price

Form DOT F 1700.7 (8-72) Reproduction of completed page authorized

This form was electrically by Elite Federal Forms Inc.

Final Report

Development of a Radar System for the Non-Destructive Measurement of Concrete Thickness

Richard Liu
Associate Professor, Principle Investigator

Jing Li and Xuemin Chen

Research Associates

Huichun Xing
Renyue Liang
Research Assistants

Project No.: TxDOT P0-4172

Conducted in Cooperation with the
Texas Department of Transportation

TxDOT Project Director: Carl Bertrand
TxDOT Project Coordinator: Ed Oshinsky
TxDOT Project Monitoring Committee: Dr. Moon Won

DISCLAIMERS

University of Houston
4800 Calhoun Rd.
Houston, TX 77204

Table of Contents

CHAPTER 1: INTRODUCTION 1
1.1 BACKGROUNDS AND OVERVIEW 1

CHAPTER 2: THE GPR SYSTEM FOR THICKNESS MEASUREMENT 3

CHAPTER 3: THE DESIGN OF TEM HORN ANTENNA 7
3.1 THE PULSE RADIATING ANTENNA 7
3.2 THE DESIGN OF THE TEM HORN ANTENNA 8

CHAPTER 4: DEVELOPMENT OF HIGH-POWER PULSE GENERATOR 13
4.1 HIGH-POWER PULSE GENERATOR 13

CHAPTER 5: SOFTWARE DEVELOPMENT 15
5.1 LAYER INFORMATION EXTRACTION AND SOFTWARE INTERFACE 15
5.2 LAYER THICKNESS CALCULATION 17

CHAPTER 6: LAB AND FIELD TESTS 21
6.1 CONSTRUCTION OF CONCRETE SLABS 21
6.2 MEASUREMENT OVER THE CONCRETE SLABS 21
6.3 FIELD TESTS ON LOOP 330 24

CHAPTER 7: CONCLUSIONS AND RECOMMENDATIONS 29
7.1 CONCLUSIONS 29
7.2 RECOMMENDATIONS 29

REFERENCES 31

List of Figures

Figure 2.1 The GPR in field test 4
Figure 2.2 The GPR measurement of a 16.5" concrete slab in lab environment 5
Figure 3.1 TEM horn antennas 9
Figure 3.2 Measured reflection coefficients of the TEM horn antenna 10
Figure 4.1 Block diagram of the pulse generator 13
Figure 4.2 Pulses generated by the two generators 14
Figure 5.1 The thickness measurement Start Up Window 16
Figure 5.2 The measured thickness and dielectric constant of the concrete pavement directly displayed on the screen 17
Figure 5.3 The geometry for the depth calculation 18
Figure 6.1(a) Concrete slab on top of an asphalt layer 21
Figure 6.1(b) Comparison of received waveforms with and without a metal plate between concrete and asphalt 21
Figure 6.2 Received signal on slab 1 22
Figure 6.3 Received signal on slab 2 22
Figure 6.4 Received signal on slab 3 23
Figure 6.5. Measured signal on Loop 330, site 1 24
Figure 6.6 Reflected wave at site 1, Loop 330 25
Figure 6.7. Measured apparent dielectric constant at site 1, Loop 330 25
Figure 6.8. Measured pavement thickness at site 1, Loop 330 25
Figure 6.9 Received Signal at site 2, Loop 330 26
Figure 6.10 Reflected waves at site 2, Loop 330 26
Figure 6.11 Measured dielectric constant at site 2, Loop 330 27
Figure 6.12 The Measured depth at site 2, Loop 330 27

List of Tables

Table 4.1 The parameters of the first pulse generator 13
Table 4.2. The parameters of the second pulse generator 14
Table 6.1 Measured thickness and apparent dielectric constant 23

CHAPTER 1: INTRODUCTION

1.1 BACKGROUNDS AND OVERVIEW

Currently, TxDOT uses two methods to measure the thickness of concrete slabs during construction. The first method involves taking and physically measuring cores every 1,000 ft. throughout the entire project. The second method involves using a calibrated stick that is pushed into wet concrete to obtain the pavement thickness. Both of these methodologies are time consuming and do not provide a continuous thickness survey of the paving project. Both of these methods necessarily assume that the pavement thickness is the same between the samples collected. A testing method that can measure pavement thickness using non-destructive techniques and is nearly continuous without the need for operator interpretation would be very beneficial. The purpose of this study is to develop a non-destructive device to measure concrete thickness continuously in the field. The device consists of four major parts: a transmitter, a receiver, a pair of antennas, and a computer control unit. The transmitter sends out a series of short pulses of high electromagnetic energy to the transmitting antenna. The receiver picks up waves, including information about the underground structure and transmitting antenna converts the pulse voltage from the transmitter into electromagnetic (EM) waves and sends the EM waves into the pavement. The receiving antenna converts the reflected waves into voltage and sends them to the receiver. The computer control unit samples and stores all the data and the processing procedures, and also controls the sequence of the measuring program. This device is based on the measurement of travel time and reflection amplitudes of a short electromagnetic pulse transmitted through a medium. When encountering dielectric discontinuities in the subsurface, part of the transmitted waves are reflected and picked up by the receiver. The received signal is then amplified and analyzed to obtain the thickness and dielectric constant of the layered media. The accuracy of the measured thickness and the dielectric constant depend on the characteristics of the device and corresponding software. In this project, we designed and implemented a ground penetrating radar (GPR) for pavement thickness measurement. The developed GPR was lab and field-tested. In the lab measurement, this

device was able to measure the concrete thickness up to 16.5 inches without steel rebars. The data inversion software was able to convert the measured signal directly into the dielectric constant and thickness readings in real time. The accuracy was satisfactory - accuracy on thickness measurement in the lab was about 0.5". This device was also taken to the field with help from Ed Oshinsky, Dr. Moon Won, and Dr. German Claros from TxDOT. The test field is located on Loop 330 in east Houston. The measured data is good but not accurate enough compared with cored thickness. We noticed that the degradation on accuracy in the field is due to the presence of the steel rebars. Due to the complexity of the device and limited time period of this project (2 months), we are only presenting major achievements in this report: system performance, design of the transverse electromagnetic wave (TEM) horn, high-power transmitter, and thickness-calculation method. The measured results using this device, in the lab and field, will also be presented.

CHAPTER 2: THE GPR SYSTEM FOR THICKNESS MEASUREMENT

The GPR system developed in this project is shown in Figure 2.1 and Figure 2.2. Inside the box shown, there is a transmitter, transmitter antenna, receiver, receiver antenna, control circuits and power supplies. The system is powered by a single rechargeable battery (4"x2"x1"), and the power consumption is about 6 watts. The output signal is digitized and displayed on a notebook computer external to the GPR system. The system's performance is as follows:

(1) Maximum Penetration Depth: 16.5" in concrete without steel rebars

The penetration depth, 16.5", is the maximum depth that has been verified using a concrete sample of this thickness; however, it is not the penetration limit of the radar system.

(2) Transmit Pulse Amplitude: 250 - 530 Vp-p

Usually the higher the transmit pulse amplitude is, the deeper the radar wave can penetrate through the concrete. However, the strength of a direct wave will also increase with the pulse amplitude and hinder the recognition of the reflected signals. The above listed amplitudes are compromised based on experimental results.

(3) Transmit Pulse Width: 5 ns (250 Vp-p) – 10 ns (530 Vp-p)

The transmit pulse width was chosen because its corresponding comprised frequencies detect resolution and penetration depth for the concrete situation. The higher frequency waves have a higher detection resolution, but decay faster while propagating in concrete. The lower frequency waves can propagate at a greater depth, but have a lower resolution.

(4) System Bandwidth: 1.3 GHz

The transmitting waves and the receiving waves are operated in the frequency range from 0 to 1.3 GHz.

(5) Receiver Window: 20 – 60 ns adjustable

Receiver window means a time interval within which the signals received by the receiving antenna are recorded in the computer. The signals from this time interval

are discarded. The receiver window is determined according to the depth expected to measure.

(6) System Clock: 100 kHz

(7) Digitization Resolution: 12 bits

(8) Antenna Type: TEM horn with resistive load

TEM horn antenna is chosen for the GPR system because it has a wide bandwidth and is easier to construct.

(9) Power Consumption: 0.5 A at 12 V (250 V transmitter), 1.5 A (530 V transmitter)

This is the total power consumed by the GPR system. A car battery provides enough energy for the system to last for a few hours.

(10) Dimension: 26"× 7.7" ×4"

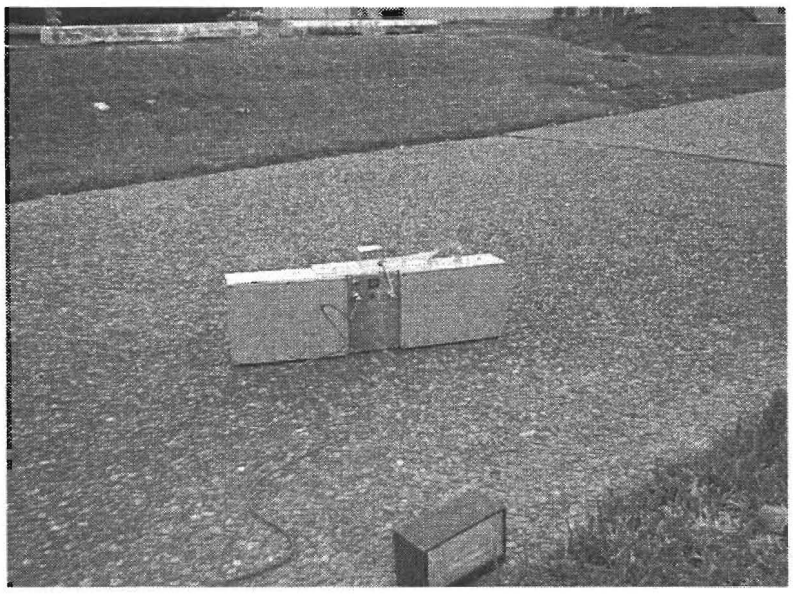

Figure 2.1 The GPR in a field test

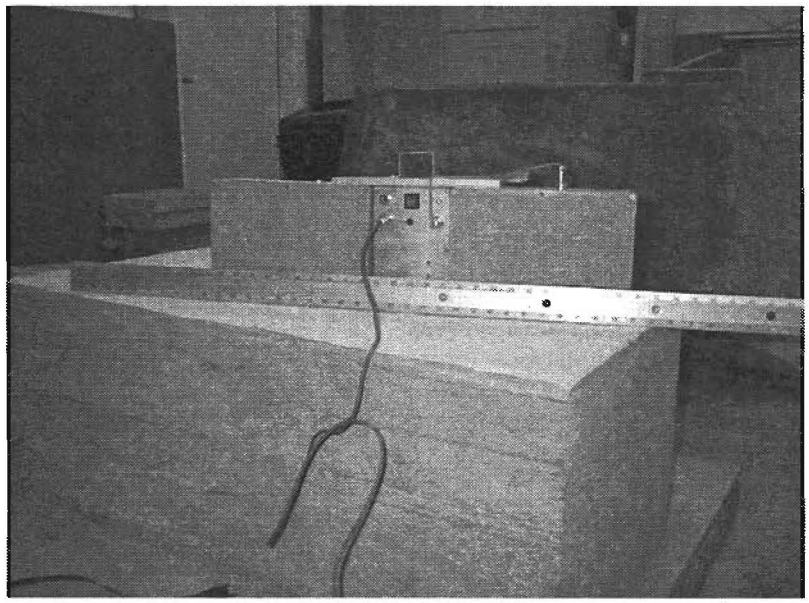

Figure 2.2. The GPR measurement of a 16.5" concrete slab in a lab environment

In Figure 2.1, the GPR was placed on top of a pavement to measure thickness in the field. In Figure 2.2, the GPR system measured the thickness of a concrete slab in the lab environment. The measurement accuracy is about 0.5" at the thickness range of 11"-18" on concrete pavement without steel rebars.

CHAPTER 3: THE DESIGN OF TEM HORM ANTENNA

3.1 THE PULSE-RADIATING ANTENNA

The transmitting antenna and the receiving antenna are important parts in the GPR system. To make the GPR system sensitive to thickness changes, the antennas should have the following characteristics:

- Minimum distortion to pulse transmission or wide bandwidth
- Direct energy to the pavement
- High radiating efficiency in a wide frequency band
- Low reflection to the feeding transmission line
- Small in size

Actually, it is impossible to make all characteristics listed above achieve their capabilities simultaneously, because some of them contradict each other, for example, minimum distortion and small in size. Theoretically, only infinitely long antennas can radiate pulse without distortion. Practical antennas are always limited in size. To make one of the antenna's characteristics perfect means sacrificing other characteristics. Hence one of the tasks in antenna design is to compromise the characteristics according to the requirements of practical applications. However, developing skills to understand and improve the antenna's specific characteristic is still the basic work in antenna design. In order to achieve the characteristics of less distortion, Wu and King [1] introduced the idea of loading the antenna with resistors. The values of the resistors increase progressively in accordance with a certain function. The purpose of using resistive loading to the antenna is to gradually decrease the strength of electric current propagating along the antenna, weakening the reflections from the open ends of the antenna. This design increases the bandwidth and reduces the reflections of the antenna, and prevents the distortion of the transmission pulse. However, the continuously resistive loading of antennas has several disadvantages: low efficiency (most power is consumed by the resistive loading instead of radiating out) input impedance of inconvenient magnitude, large dimensions, and difficulty of mechanical construction. E. A. Theodorou [2] proposed another idea: by varying the characteristic impedance

smoothly throughout the antenna structure, with the characteristic impedance at two ends of the antenna matching that of the feed line and the free space, respectively, the bandwidth can also be increased without much resistive loading. Kurt L. Shlager [3] improved the design by smoothly bending the antenna plate to reduce the aperture of the antenna, so that the reflections from the open ends of the antenna are further reduced. Though Theodorou and Shlager's design obtains a wide bandwidth without applying progressively resistive loading to the antenna, the structure of the antenna has a small ratio of the radiation aperture over the length of the antenna (approximately 1/5). Unfortunately, the radiation efficiency of an antenna is proportional to the size of its radiation aperture. If the aperture of the antenna is enlarged to some width to provide acceptable radiation efficiency, the size of the antenna on the other dimension has to be enlarged five times to maintain the antenna's balance. Hence, Theodorou and Shlager's design is not a good choice for the GPR radar due to its large size.

In this study, we increased the antenna bandwidth by shaping the plates of the antenna in two dimensions and introduced resistive loading only at the end of the antenna. Details regarding the design and the performance of new antennas will be given in the following section.

3.2 THE DESIGN OF THE TEM HORN ANTENNA

Since the antenna characteristics (such as radiation pattern and input impedance) vary with the surrounding environment, the application scenario of the GPR is also an important factor to the design of GPR antennas. In the case of thickness measurement of concrete pavement, the pavement's reaction to the antennas must be taken into account in the antenna design. Based on theoretical and experimental results, we developed a new TEM horn antenna. The antenna is made of two identical metal platesthat are specially shaped in both transverse and longitudinal directions. Figure 3.1 shows the structure of the plate.

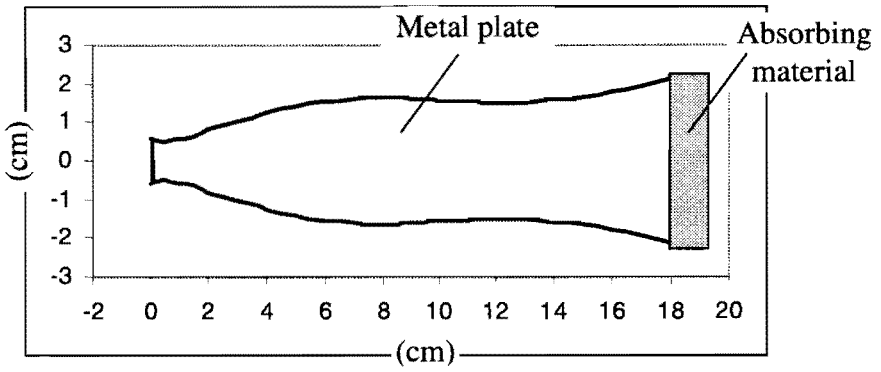

(a) Top view

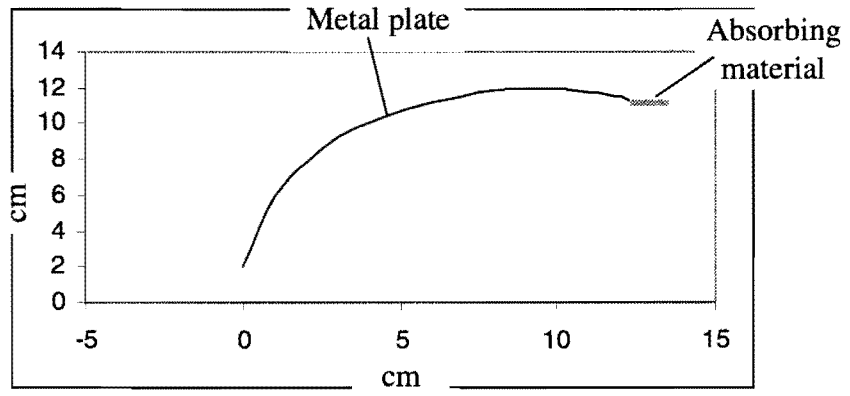

(b) Side view

Figure 3.1 TEM horn antennas

The curved plate has a total length of 18 cm. The shadowed area at the end of the plate is a piece of absorbing material, a resistive loading to the antenna to reduce the reflection at the two ends of the antenna. By adjusting the shape and curvature of the plate, the reflections from the antenna can be made acceptably small. Figure 3.1 shows one of the optimized shapes.

By adding proper absorbing materials at the terminal end of the antenna, the reflections from the antenna, in the desired frequency band, can be further reduced. Figure 3.2 gives the measured reflection coefficients (S_{11}) of the designed antenna within the frequency range of 50 MHz to 500 MHz. Here, S_{11} represents the ratio of the strength of input

signals over the strength of the signal reflected from the antenna. The smaller the S_{11} of an antenna, the less the antenna reflects the input energy, and the more the antenna radiates the input energy out into space. Small S_{11} is what we expect, and the smaller the better. However, S_{11} cannot be made arbitrarily small, because the size and structure of the antenna confine it. For the GPR system we constructed, -12dB is an acceptable value for S_{11}. The frequency range (50 MHz to 500 MHz) is chosen to view the reflection coefficient of the antenna, since it already covers the main bandwidth of the transmitted electromagnetic pulse of the GPR system. The components out of this frequency range are small enough to be neglected.

One feature of the designed antenna is its compact size. When a 6ns electromagnetic pulse propagates in free space, it occupies a space of 1.8m in the propagation direction. The space occupied by a pulse along its propagation direction is referred to as space span here. Compared with the space span of the transmitted pulse, the length of the antenna plate shown in Figure 3.1, is only 1/10 of the pulse span. The relative size of the antenna is small, and a satisfactory reflection performance is also obtained in the frequency band of 50-500 MHz as shown in Figure 3.2. The horizontal axis shows frequency in MHz, and the vertical axis shows magnitude of the reflection in dB.

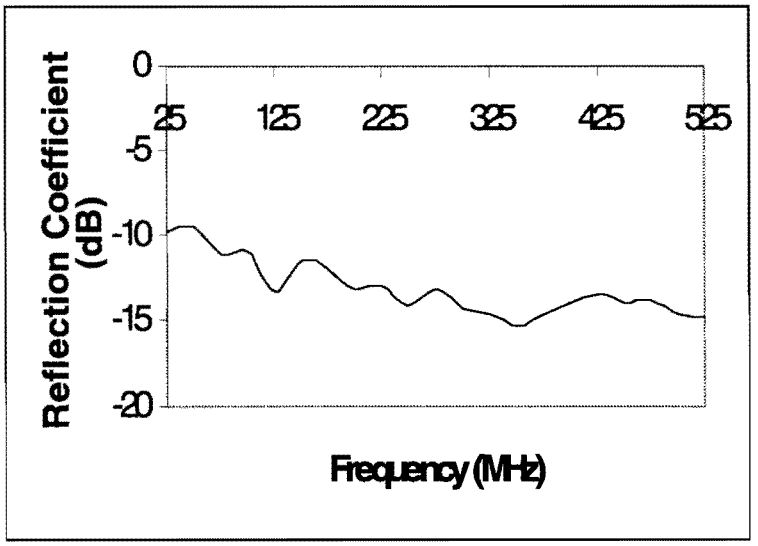

Figure 3.2 Measured reflection coefficients of the TEM horn antenna

In pavement detection, the ripples on a received waveform are the contributions of direct waves (from transmitting antenna directly propagating to the receiving antenna), the reflections from antenna ends, the reflections from the pavement surface, the reflections from the lower interface between the pavement and asphalt, and so on. One important task in pavement detection is the recognition of the exact ripple that represents the reflection of the lower interface of pavement from a large group of unnecessary ripples. Improved antenna characteristics can help reduce those unnecessary ripples and make the expected ripple clearer. The resolution and depth of penetration can both be improved.

CHAPTER 4: DEVELOPMENT OF HIGH-POWER PULSE GENERATOR

4.1 HIGH-POWER PULSE GENERATOR

Higher pulse power is helpful in achieving a greater penetrating depth. In order to obtain a higher resolution and deeper penetrating depth at the same time, two high-power pulse generators were developed for this project. The block diagram of the first pulse generator is shown in Figure 4.1. The measured parameters of the generator are given in Table 4.1.

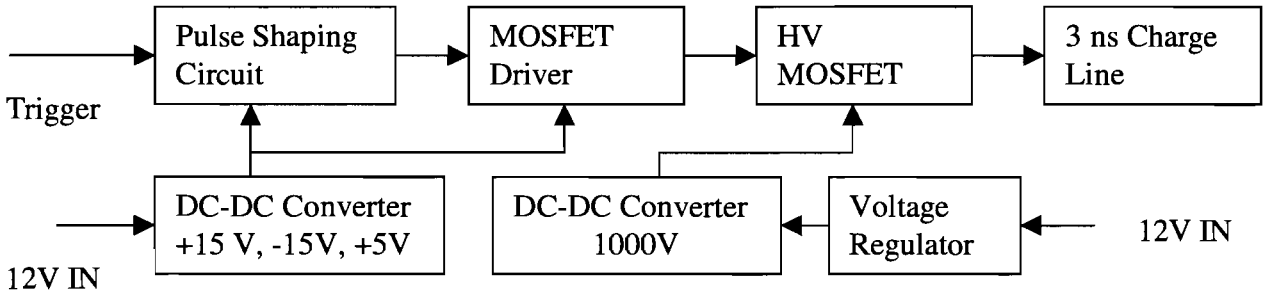

Figure 4.1. Block diagram of the pulse generator

Table 4.1 The parameters of the first pulse generator

Pulse Voltage	Pulse Width	Repetition Rate	Power Supply	Instant Power
530V	10ns	3 kHz	DC 12V, 0.5A	5,618 Watt

The second pulse generator, which is designed for high accuracy measurement, has less power than the first one. The second pulse generator's diagram is similar to the first one, only the parameters of electronic elements differ. The measured parameter of the second pulse generator is shown in Table 4.2.

Table 4.2. The parameters of the second pulse generator

Pulse Voltage	Pulse Width	Repetition Rate	Power Supply	Instant Power
250V	5ns	150 kHz	DC 12V, 0.15A	1,250 Watt

The pulses produced by the two generators are displayed in Fig. 4.2. One generator is an alternative of the other. Either the first generator or the second generator will be used depending on the situation of practical applications.

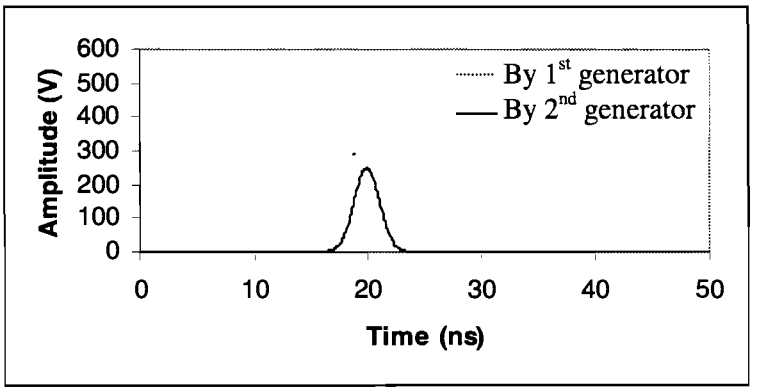

Fig. 4.2 Pulses produced by the two generators

CHAPTER 5: SOFTWARE DEVELOPMENT

5.1 LAYER INFORMATION EXTRACTION AND SOFTWARE INTERFACE

So far we have developed software capable of sampling GPR signal traces and storing them on a computer. In this study, we devoted our efforts to the layer information extraction from the measured GPR data. The received GPR signals contain both direct waves and reflected waves. The reflected waves from the bottom of the concrete pavement are the most useful information. If the reflections are identifiable from the tails of direct waves, they can be easily detected from the measured waveforms. The software to search and identify the reflection-related humps was developed in this project. Lab tests discussed in Chapter 6 show that the software is reliable and effective.

The reflections from the bottom of a thick concrete slab are usually very weak. There may be no obvious reflection-related humps on the GPR waveform. However, the reflection will make the overall received signal discontinuous. One way to address this problem is to use wavelet functions to simulate the direct waves. By subtracting the simulated direct wave from the total measured signal, the interference of the direct waves can be reduced, and the reflection-related humps can be singled out. According to the characteristics of the developed GPR system, the following wavelet function estimates the direct wave:

$$f(t) = A\exp[-(\frac{t-t_0}{\alpha})^2]\cos[\beta(t-t_0)] \qquad (5-1)$$

We have found that the first part of the measured waveform (before the first largest peak), which represents the directly coupled waves and reflections inside the GPR, do not change much regardless of the change in application background. Hence this part of the waveform can be used to determine the coefficients of the chosen wavelet function. Once the direct waves are simulated, the layer information can be obtained by subtracting the direct waves from the total signals.

The performance of this technique is described in Chapter 6. The data interpretation is in real time and fully automatic. No operator experience is needed. Figure 5.1 shows the initial window on the laptop computer screen. An operator types in the name of the output file in the upper right corner of the window and runs the software by clicking on the "Start" button. Figure 5.2 shows the GPR output data. This data objectively shows the thickness and the measured dielectric constant without any guessed values. The techniques to measure, record, and display location information of measurements will be developed in the next step.

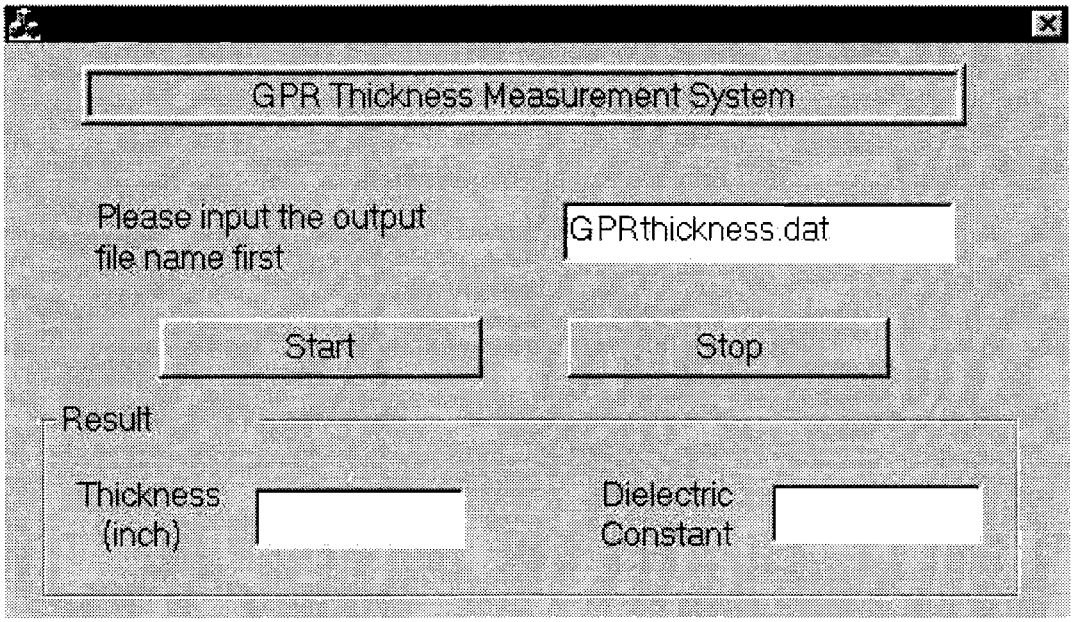

Figure 5.1 The thickness measurement Start Up Window

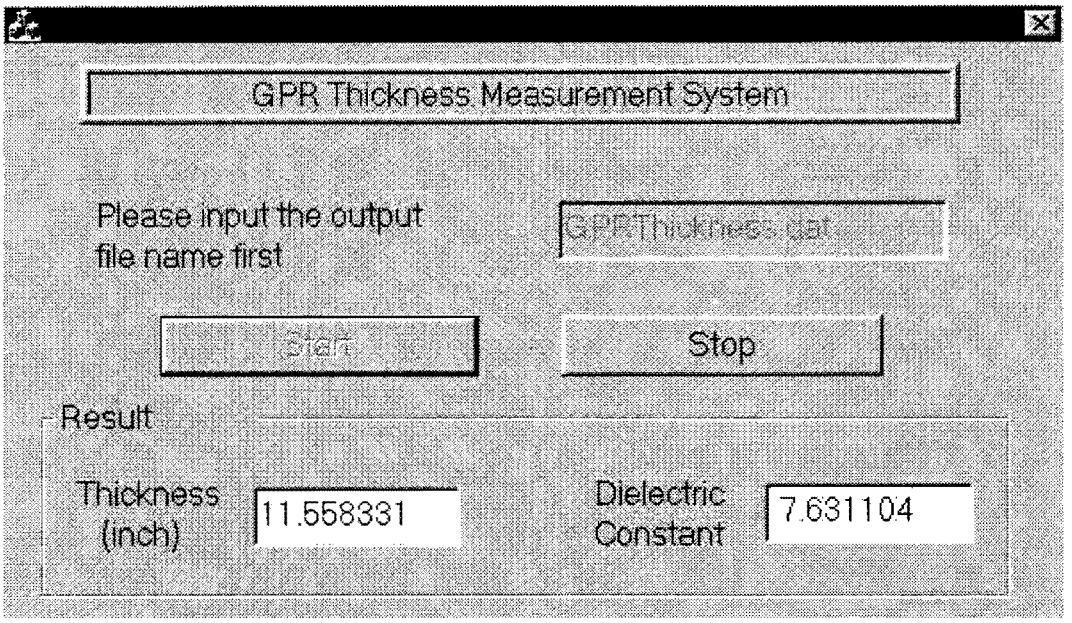

Figure 5.2. The measured thickness and dielectric constant of the concrete pavement displayed on the screen

5.2 LAYER THICKNESS CALCULATION

Once the reflected waves are identified, the propagation time and the amplitude of the reflected wave can be found and used to calculate the thickness and dielectric constant of the pavement. However, the amplitude of the reflected wave is difficult to accurately measure in practical applications. Only the measurement of time information is reliable. Here, a new mathematical model, which only requires time information, has been developed for both thickness and dielectric constant calculation.

This model is based on the bi-static radar system. In most GPR data interpretation algorithms, seismic data processing methods have been utilized in processing GPR data [4, 5, 6, 7, 8, 9, 10]. We noticed that the effect of a significant difference between the seismic sensing and GPR detection has not been properly addressed in the direct application of seismic methods to GPR data interpretation. The seismic sensors are all

buried underground, while the GPR antennas are above the ground surface. The air-concrete interface, which does not need to be taken into account in seismic processing, is introduced in GPR detection. This fact caused the electromagnetic rays from the GPR to take a different propagation path; therefore, ray path searching must be included in the calculation algorithm.

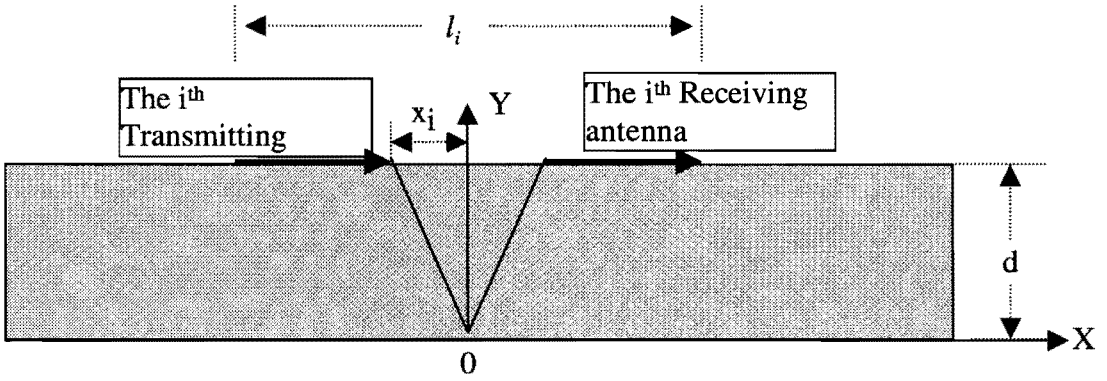

Figure 5.3. The geometry for the depth calculation

Figure 5.3 describes the geometry for the depth calculation. Since the rays must take the shortest path by Fermat's Law, they may not go down directly from the transmitting antenna to the reflection point at "0". We suppose the rays penetrate the interface at a point x_i away from the y-axis. In this case, two equations can be obtained:

$$\begin{cases} \sqrt{\varepsilon_r(x_i^2+d^2)} - x_i = u_0 \Delta t_i / 2 \\ \dfrac{\partial}{\partial x_i}[2\sqrt{\varepsilon_r(x_i^2+d^2)} + 2(l_i - x_i)] = 0 \end{cases} \tag{5.1}$$

Where, d and ε_r are the thickness and dielectric constant of the concrete pavement, and l_i is the distance between the transmitting and the receiving antennas. Δt_i is the time interval between the direct wave and the reflected wave from the lower interface. For bi-static radar, a series of equations like Equation (5.1) can be established. The

unknowns in the equations are d, ε_r and x_i, (i = 1,2,3...). By solving these equations, the thickness and apparent dielectric constant of the pavement can be obtained.

If x_i is found to be the value of $l_i/2$, the results are coincided with that of seismic waves. However, x_i never takes the value of $l_i/2$ in the cases we investigated. This implies that GPR waves take different paths from that of seismic waves. Since Equations (5.1) used the actual ray path of GPR waves, the estimated thickness from measured reflection data agrees with the real thickness closely. For more information see Chapter 6, Lab and Field Tests.

CHAPTER 6: LAB AND FIELD TESTS

6.1 CONSTRUCTION OF CONCRETE SLABS

To verify both the hardware and software algorithms of the developed GPR system, three concrete slabs were built in the laboratory. The actual thicknesses of the three slabs are 9.5", 11", and 16.5". One of the slabs was placed on a layer of asphalt to simulate the real pavement situation. The geometry of the slab is shown in Figure 6.1 (a). The other two slabs are placed on wood bars 4" above the ground.

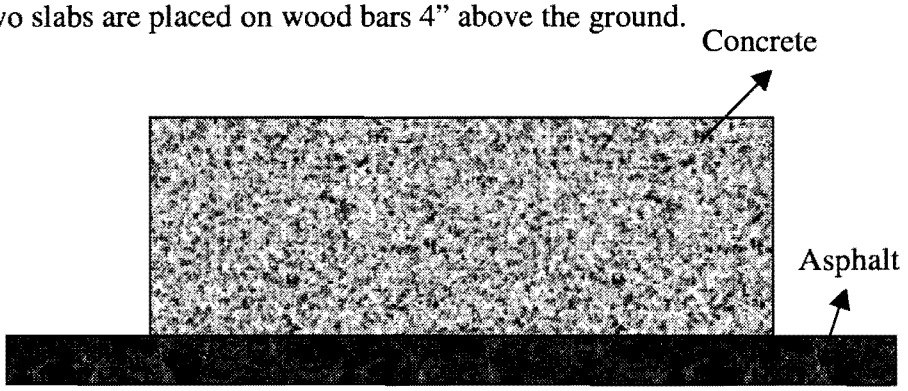

Fig. 6.1 (a) Concrete slab on top of an asphalt layer

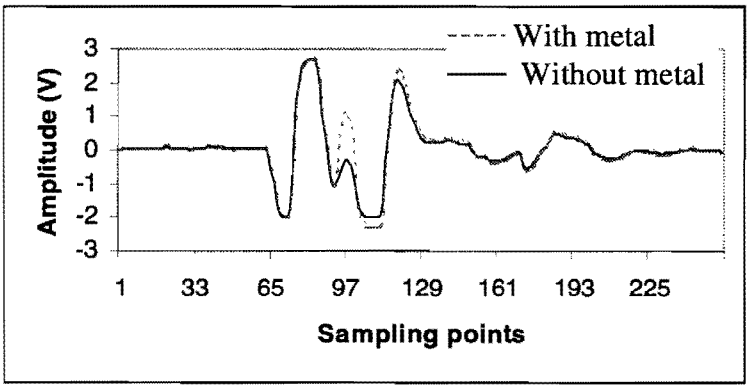

Fig. 6.1 (b) Comparison of received waveforms with and without a metal plate between concrete and asphalt.

6.2 MEASUREMENT OVER THE CONCRETE SLABS

The developed device was tested in the laboratory using the three constructed concrete slabs. The first test was conducted on slab 1, (actual thickness 9.5"). The second and third tests were carried out on slab 2 (11" thick) and slab 3 (16.5" thick). A

hundred runs of measurements were done over each slab. Since the recorded waveforms on a slab are identical, here only one waveform is chosen and displayed from each group. Figure 6.2 is one of a hundred identical waveforms recorded over slab 1. Figure 6.3 is a trace recorded on slab 2, and Figure 6.4 is recorded on slab 3.

The humps denoted in Figure 6.2 through Figure 6.4 are verified to be the reflected waves from the bottom surface of the slabs. When a piece of metal plate is inserted in between the concrete slab and the underneath asphalt, the amplitudes of the humps will change sharply, while the other area of the waveform remains unchanged. This shows that the humps are the expected reflections from the interface between the concrete slab and the asphalt layers.

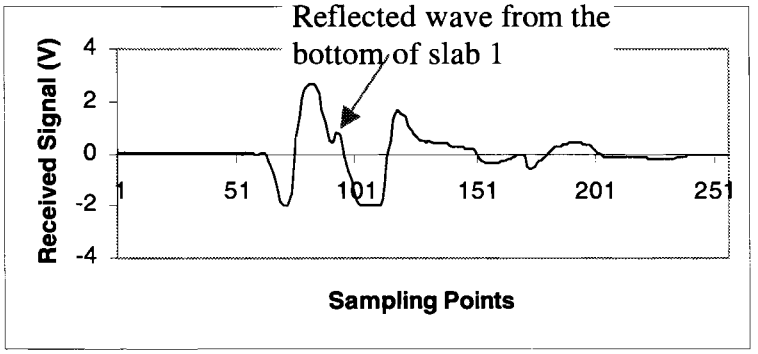

Figure 6.2 Received signal on slab 1

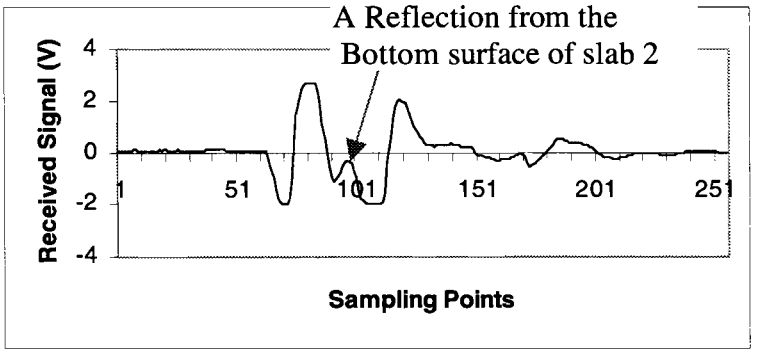

Figure 6.3 Received signal on slab 2

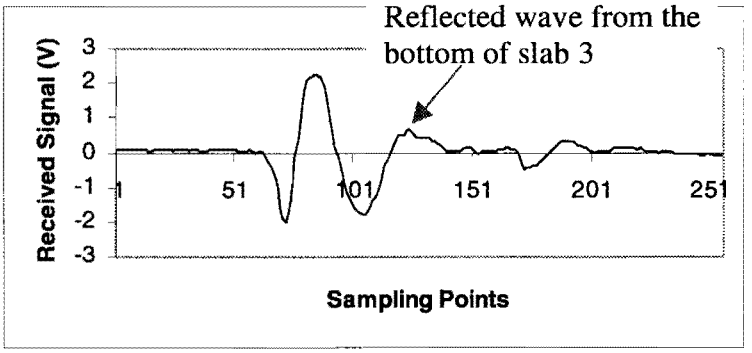

Figure 6.4 Received signal on slab 3

According to the received waveforms, the thickness and the apparent dielectric constant can be calculated using the algorithms described in Chapter 4. The calculated results are given in Table 6.1.

Table 6.1 Measured thickness and apparent dielectric constant

	Slab 1	Slab 2	Slab 3
Measured Dielectric Constant	7.78	7.47	8.35
Measured Thickness	11.02"	9.35"	16.8"
Actual Thickness	11"	9.5"	16.5"
Standard Deviation	4.85%	5.2%	4.23%

Here standard deviation is defined as:

$$\sigma = \frac{\sqrt{\frac{1}{100}\sum_{i=1}^{100}(h_i - H)^2}}{H} \qquad (5-2)$$

where h_i is one of 100 measured thickness and H is the average of the 100 measurements. The measured thickness of the three slabs are very close to the their actual values. The developed device has been tested and verified to measure the thickness of concrete slabs with satisfactory accuracy.

6.3 FIELD-TESTS ON LOOP 330

After laboratory experiments, field tests were also conducted. Figure 6.5 is one of the measured signals on a section of the freeway on Loop 330 in southeast Houston. Two sites were selected for the measurement. Site 1 is located on the southbound side of Loop 330, and Site 2 is on the northbound side of Loop 330. At Site 1, a core was taken and the thickness of the core was ruler-measured. The thickness of the core is about 10.5". Steel rebars were found inside the pavement. The diameter of the steel is 5/8" transverse and 3/4" longitudinal. The steel rebars are 4" above the base. Since the test sections are relatively new, the moisture contents are much higher than the concrete slabs in the Lab environment. The reflected waves from the concrete-asphalt interface are very weak with respect to the direct waves. Sometimes no obvious humps are visible on the waveforms. However, the radar traces show some irregularly changing points on the waveforms. These irregularly changing points are caused by the superposition of the direct wave and the reflected wave from the interface. The position, where an irregularly changing point occurs, should correspond to the arrival time of the reflected wave. After subtracting the simulated direct wave from the measured waveform (Figure 6.5), the reflected waves do emerge at those irregularly changing points, as shown in Figure 6.6.

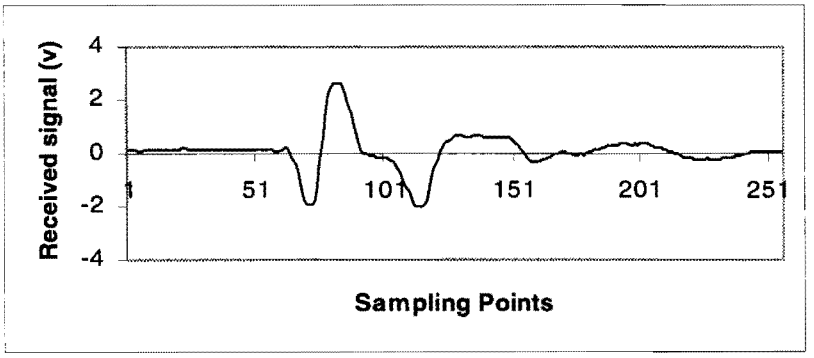

Figure 6.5. Measured signal on Loop 330, Site 1

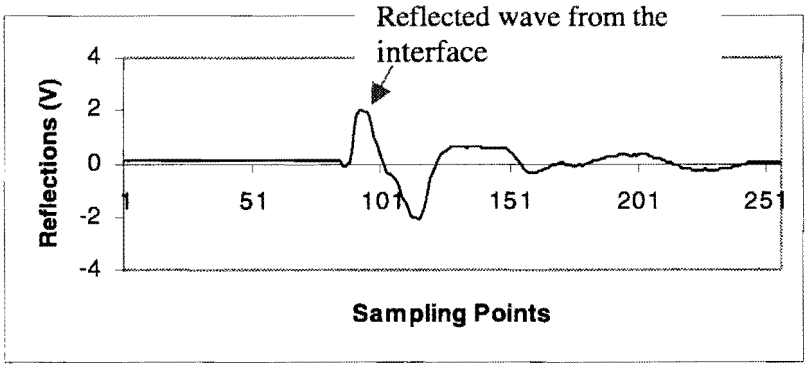

Figure 6.6 Reflected wave at Site 1, Loop 330

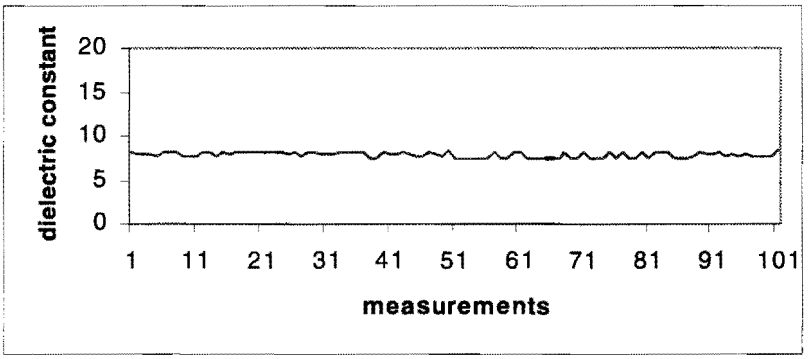

Figure 6.7. Measured dielectric constant at Site 1, Loop 330

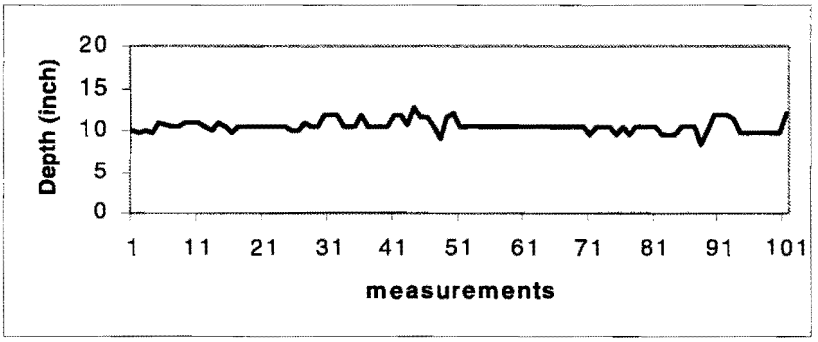

Figure 6.8. Measured pavement thickness at Site 1, Loop 330

By learning the arrival time of the reflected wave from the interface, the thickness and dielectric constant of pavement on Loop 330 (Site 1) can be calculated by solving the

equations explained in Chapter 4. Figure 6.7 and Figure 6.8 are the results of 100 repeated measurements.

Repeating the procedures used at Site 1, similar results were obtained at Site 2 on Loop 330. Figure 6.9 is one of the waveforms recorded at Site 2 on Loop 330. Figure 6.10 is the reflection signal indicating the propagation time of the reflected wave. Figure 6.11 and Figure 6.12 are the results of 33 repeated measurements on Loop 330 at Site 2.

The results at both sites of Loop 330 are very close to the actual thickness measured by coring (10.5 inches).

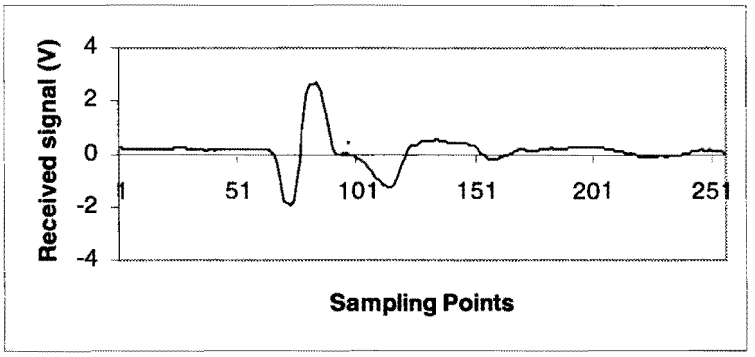

Figure 6.9 Received Signal at Site 2, Loop 330

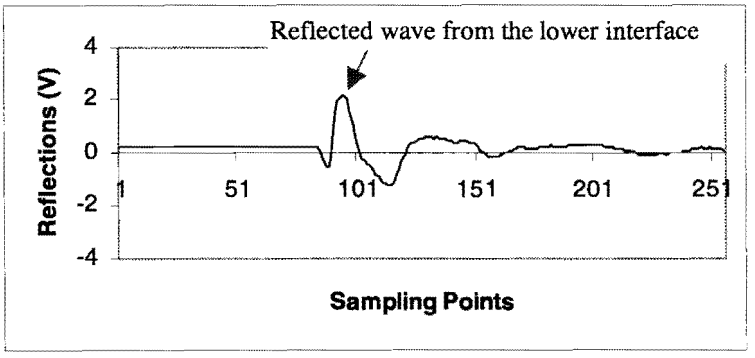

Figure 6.10 Reflected waves at Site 2, Loop 330

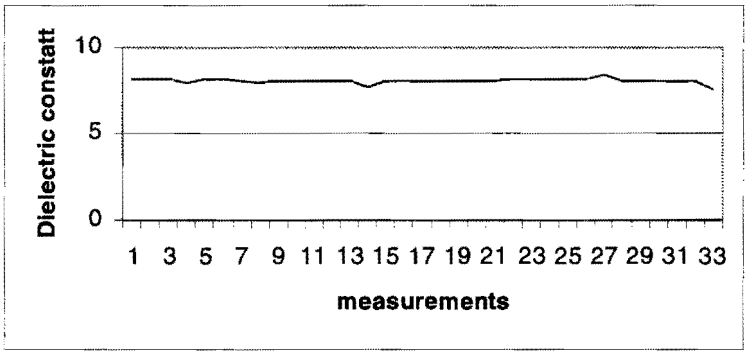

Figure 6.11 Measured dielectric constant at Site 2, Loop 330

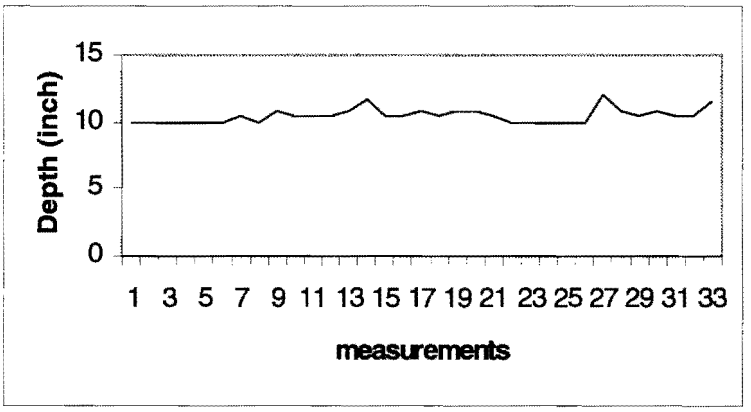

Figure 6.12 The Measured depth at Site 2, Loop 330

CHAPTER 7: CONCLUSIONS AND RECOMMENDATIONS

7.1 CONCLUSIONS

This project has been very successful considering the two-month life span and the product delivered. The developed GPR hardware and software can measure the concrete thickness automatically. The prototype GPR and software programs were lab and field-tested. The test results show that this system can measure the concrete thickness up to 16.5". In the case where steel rebars exist, this system can also detect the thickness with small modifications.

7.2 FUTURE WORK

The prototype can be quickly converted to a field measurement tool if the system is properly modified. The researchers recommend the following future work:

1. Modify the hardware and software, such as increasing the sampling points and dynamic range in hardware and removing influence of rebars in software, so that the concrete thickness can be accurately measured with or without steel rebars
2. Incorporate a distance measurement device into the system to measure the positions
3. Modify the device to measure thickness of asphalt pavement

REFERENCES

[1] Wu, T. T., and R.W.P. King, "The Cylindrical Antenna with Non-reflection Resistive Loading," *IEEE Trans.* AP-13, pp.369-373, (1965).

[2] Theodorou, E.A., M. R. Gorman, P. R. Rigg, and F.N. Kong, "Broadband Pulse-optimized Antenna," *IEE Proc.* Vol.28, pt. H. pp. 124-130, (June 1981).

[3] Shlager, Kurt L., G. S. Smith, and J. G. Maloney, "TEM Horn Antenna for Pulse Radiation: An Improved Design," *Microwave and Optical Technology Letters,* Vol.12, No.2, pp. 86-90, (June 1996).

[4] Walker, P.D., and M. R. Bell, "Subsurface Permittivity Estimation From Ground-Penetrating Radar Measurements," *IEEE International Radar Conference,* pp. 341-346, (2000).

[5] Ralston, J.C., D. W. Hainsworth, and R. J. Mcphee, "Application and Ground Penetrating Radar for Coal Thickness Measurement," *IEEE TENCON-Speech and Image Technologies for Computing and Telecommunications,* pp. 835-838, (1997).

[6] Cai, J. and G. A. McMechan, "Ray-based Synthesis of Bistatic Ground-Penetrating Radar Profiles," *Geophysics,* Vol. 60, No. 1, pp. 87-96, (1995).

[7] Spagnolini, U., "Permittivity Measurements of Multilayered Media With Monostatic Pulse Radar," *IEEE Transaction on Geoscience and Remote Sensing,* Vol. 35, No. 2, pp. 454-463, (March 1997).

[8] Huang, Y. and D. Parsons, "A Time Domain Approach for Measuring the Dielectric Properties and Thickness of Walls of a Building."

[9] Fisher, E., G. A. McMehan, and A. P. Annan, "Acquisition and Processing of Wide-aperture Ground-Penetrating Radar," *Geophysics,* Vol. 57, pp. 494-504, (1992).

[10] Fisher, E., G. A. McMehan, A. P. Annan, and S. W. Cosway, "Examples of Reverse-Time Migration of Single-Channel Ground-Penetrating Radar Profiles," *Geophysics,* Vol. 57, pp. 577-586, (1992).